RESEARCH ARTICLE

In-silico Validation of Pyrazolone Derivatives as the Potent Scaffold for Modulating Protein Abnormalities Associated with Parkinson's Disease

Harsha Ashtekar[1*], Prarambh S. R. Dwivedi[1], Natasha Aggarwal[2], Zeena Fernandes[1], Nimmy Varghese[1]

[1]*Department of Pharmacology, NGSM Institute of Pharmaceutical Sciences(NGSMIPS), Nitte (Deemed to be University), Mangalore, India*

[2]*Department of Pharmaceutical Chemistry, Yenepoya Pharmacy College and Research Center, Yenepoya (Deemed to be University), Mangalore, India*

Received: 08th January, 2023; Revised: 14th February, 2023; Accepted: 04th March, 2023; Available Online: 25th March, 2023

ABSTRACT

Aim: We explored pyrazolone derivatives for anti-Parkinson's activity using *in-silico* tools to identify novel lead hits against Parkinson's disease.

Background: Parkinson's disease is the most predominant neuronal degenerative disorder, caused by protein aggregation and dopamine imbalance. The available therapeutic agents on prolonged exposure lead to severe adverse effects and provide only symptomatic relief. Therefore, it is a need for novel drug molecules that would modulate the disease condition.

Objectives: To identify novel hit molecule for a sequence of molecules designed using pyrazolone as a parent moiety by computer-aided drug design techniques.

Materials and Methods: Derivatives are generated by various substituted functional groups and further, pharmacokinetic profile, the biological spectrum, adverse drug effect, molecular docking, molecular dynamic, and MMPBSA evaluation was performed.

Results: Thirty-four compounds follow a pharmacokinetic profile. 15 compounds were predicted to possess a positive central nervous system activity score. The compounds C13, C12, C14, A1, C9, and C7 possessed the highest binding affinity of -7.81, -3.15, -8.49, -3.43, -6.09, and -2.77 kcal/mol with various targets involved in Parkinson's disease. Compound C13 exhibit ed highest binding score of -9.78 kcal/mol formono amino oxidase-B.

Conclusion: From our investigations, we hope that novel substituted pyrazolone derivatives can act as an assuring virtual hit molecule for developing anti-Parkinson's agents. These predictions obtained *via in-silico* techniques could aid the development of pharmacological inhibitors for Parkinson's disease.

Keywords: *In-silico*, Molecular docking, Molecular simulation, Mono amino oxidase, Parkinson's disease, Pyrazolone.

International Journal of Drug Delivery Technology (2023); DOI: 10.25258/ijddt.13.1.01

How to cite this article: Ashtekar H, Dwivedi PSR, Aggarwal N, Fernandes Z, Varghese N. *In-silico* Validation of Pyrazolone Derivatives as the Potent Scaffold for Modulating Protein Abnormalities Associated with Parkinson's Disease. International Journal of Drug Delivery Technology. 2023;13(1):1-9.

Source of support: Nil.

Conflict of interest: None

INTRODUCTION

Parkinson's disease (PD) is considered most predominant neuronal degenerative disease in elderly patients and is clinically incurable.[1] PD is caused by degeneration of dopaminergic neurons at substantia-nigra pars-compacta (SNPC) which leads to the motor and non-motor dysfunctionality; it affects about 1–2% of geriatrics population, and its prevalence is proclaimed to increases with age.[2,3] The current pharmacotherapy of Parkinson's disease aims to improve its symptoms, involving the use of levodopa as a gold standard along with mono-amino-oxidase-B inhibitors (MAO-B), Catechol O-methyl transferase inhibitors (C-O-MT), and dopamine (DA) agonists.[4] Though, at present, there is no standard treatment guideline for curing PD, offering the necessity to identify novel anti-Parkinson's drugs.

Recently synthetic medicines have gained significant importance over traditional herbal medicines due to their substantial potency and cost-effectiveness. Pyrazolone is a derivative of 3-pyrazoline containing a lactam cyclic pentane with dinitrogen and one ketonic group.[5] The pyrazolone derivatives are known to be used for the treatment of

**Author for Correspondence: hrshshtkr2@gmail.com*

inflammation, Lou Gehrig's disease and are known to be antipyretic and analgesic. Moreover, pyrazolone derivatives are also reported to own anti-cancer, anti-depressant, and *in-vitro* MAO-B inhibitory effects.[6-8]

In the current drug discovery scenario, *in-silico* tools play a prominent role, initially in identifying a lead hit among numerous compounds. Absorption; distribution; metabolism, and elimination (ADME) activity of a compound helps us to calculate the pharmacokinetic profile of a test agent. It may be used as a parameter to screen compounds to identify a lead hit.[9] It is evident that a drug molecule modulates multiple proteins, which may or may not be involved in the pathogenesis of targeted disease; modulation of anti-targets leads to side effects. In addition, if a drug targets multiple proteins involved in the pathogenesis of the disease, it may possess greater efficacy than mono-targeted drugs. With regard to this, we have identified eight targets involved in the pathogenesis of PD *i.e.* tumor necrotic factor receptor associated protein 1 (TRAP-1), mono amino oxidase-B (MAO-B), DA receptor I (DAI), DA receptor II (DAII), β-cell lymphoma extralarge (Bcl-xL), regulator of apoptosis (BAX), caspase 3 (CASP3) and caspase 9 (CASP9).[10,11] Hence, in the present study, we designed to discover lead hit molecule from substituted pyrazolones against Parkinson's disease by utilizing various *in-silico* tools like molecular docking, dynamic simulation, and ADME profile.

MATERIALS AND METHODS

ADME Prediction

The ADME profiling of pyrazolone derivatives was performed *via* the QikProp module of Schrodinger to predict nine physically significant and pharmacological characteristics viz. molecular weight, drug-likeness score, CNS activity score, dipole moment, number (no.) of hydrogen bond acceptor, QPlog O/W, no. of likely metabolic reaction, no. of Lipinski violations, and percent human oral absorptivity.[12]

Biological Activity and Adverse Reaction (ADR) Prediction

The biological spectra of the pyrazolone derivatives were predicted using the prediction of activity spectra for substance (PASS) online prediction tool (http://www.way2drug.com/passonline/) with a limit of pharmacological activity (Pa) greater than pharmacological inactivity (Pi).[13] The biological spectra were made specific to Parkinson's disease *via* the keywords Bcl-xl, Bax, catechol-o-methyl transferase, and mono amino oxidase inhibitors. ADVERPred (http://www.way2drug.com/adverpred/) webserver was utilized to predict the ADR which may be caused by the test agents when administered to humans.[14] The pharmacological activity more significant than pharmacological inactivity was considered a parameter to predict the adverse effects.[15,16]

Molecular Docking

Ligand Preparation

Important substitution in arrangement of ligands were constructed using the Chemsketch software (Figure 1).[17] The LigPrep module was used to prepare ligands for docking. Ligands were converted into 3D configurations via ionization, tautomerism, energy minimization, and geometry optimization. Further, ionization and tautomeric conditions were created at pH ranging from 6.8 to 7.2 using Epik-module.[18]

Preparation of Protein

The X-ray crystallographic structure of the targets comprising co–crystalline-ligand, hydro molecule, metallic ions, and co-factors were retrieved from protein data bank (Figure 2). The protein preparation tool of Schrodinger group 2019-2 was exhibited to prepare proteins.[19] Potential states of ionization for the het-atoms in the target were produced, and state with the highest stability was chosen. Minimizing the energy of protein was accomplished by optimized-potentials-for-liquid-simulations-3 (OPLS-3) force field.[20]

Receptor Grid Set to Generation

A receptor grid for protein-ligand docking was generated via the site map module in the Schrodinger suite glide. The binding site possessing the largest volume was considered to form a grid where docking is to be performed. The proteins possessing a co-crystallized structure were not subjected to site map generation, and the residues involved in the complex were considered to generate a grid.[21] Altogether ligands were docked in created grids respectively.[22]

Glide ligand docking

The protein-ligand docking was performed after receptor grid preparation the active site via the glide program of Schrodinger software 2019-2. Docking performed in a versatile mode of docking that mechanically generated conformations for every ligand input, via extra precision mode. The ligand owning lowest glide generated scores was used to envisage the protein-ligand complex interaction by the Glide module's-XP visualizer, with a 2-dimentional appearance of the interactions were extracted.

Molecular Dynamic (MD) Simulation

MD simulation performed for best protein-ligand interaction (C13 with MAO-B) via GROMACS 2021. The pdb2gmx tool *via* the Charmm36 force field (February 2021) was used to generate topology of the protein; ligand topology was generated using an external CGenFF server. Dodecahedron case of 10 Å was formed around the water filled complex that was neutralized by addition of ions. The steepest descent algorithm was applied for a maximum of 50000 steps for energy minimization with a verlet cut-off scheme. The LINCS algorithm was used for constraining the atoms, and particle Mesh Ewald (PME) was used to equilibrate the electrostatic forces. The isotropic C-rescale and V-rescale algorithms were used to stabilize the pressure and temperature of the system (300 K). The simulation was accomplished for 20000 picoseconds, and energies were saved at every 20 ps. After the completion of the MD run, various modules of GMX were utilized to analyze the results.[23]

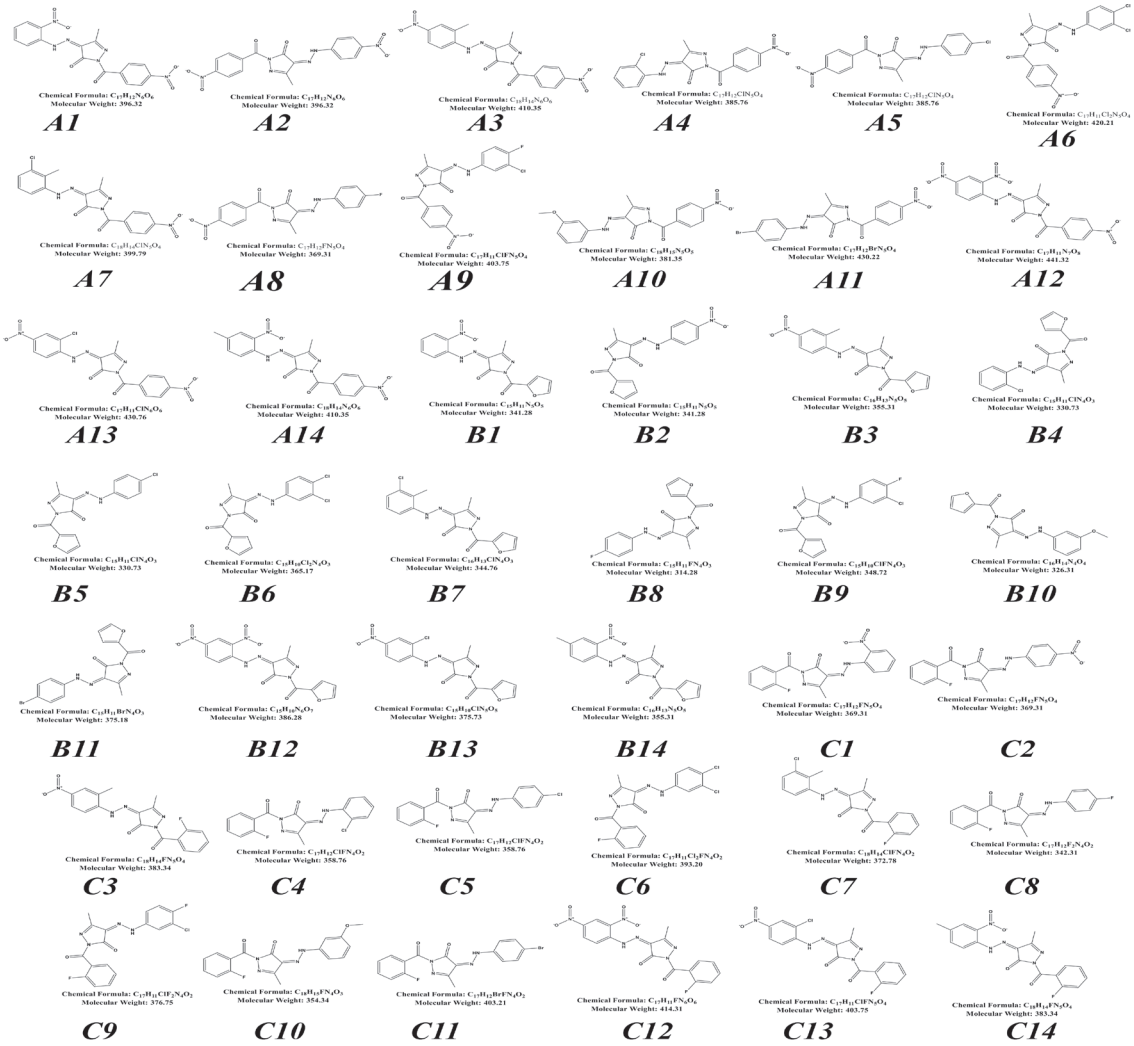

Figure 1: 2D structure of Pyrazolone derivatives along with their chemical formula and molecular weight
A1: (4Z)-3-methyl-1-(4-nitrobenzoyl)-1H-pyrazole-4,5-dione 4-[(2-nitrophenyl)hydrazone]; ***A2:*** (4Z)-3-methyl-1-(4-nitrobenzoyl)-1H-pyrazole-4,5-dione 4-[(4-nitrophenyl)hydrazone]; ***A3:*** (4Z)-3-methyl-1-(4-nitrobenzoyl)-1H- -4,5-dione 4-[(2-methyl-4-nitrophenyl)hydrazone]; ***A4:*** (4Z)-3-methyl-1-(4-nitrobenzoyl)-1H-pyrazole-4,5-dione 4-[(2-chlorophenyl)hydrazone]; ***A5:*** (4Z)-3-methyl-1-(4-nitrobenzoyl)-1H-pyrazole-4,5-dione 4-[(4-chlorophenyl) hydrazone]; ***A6:*** (4Z)-3-methyl-1-(4-nitrobenzoyl)-1H-pyrazole-4,5-dione 4-[(3,4-dichlorophenyl)hydrazone]; ***A7:*** (4Z)-3-methyl-1-(4-nitrobenzoyl)-1H-pyrazole-4,5-dione 4-[(3-chloro-2-methylphenyl)hydrazone]; ***A8:*** (4Z)-3-methyl-1-(4-nitrobenzoyl)-1H-pyrazole-4,5-dione 4-[(4-fluorophenyl)hydrazone]; ***A9:*** (4Z)-3-methyl-1-(4-nitrobenzoyl)-1H-pyrazole-4,5-dione 4-[(3-chloro-4-fluorophenyl)hydrazone]; ***A10:*** (4Z)-3-methyl-1-(4-nitrobenzoyl)-1H-pyrazole-4,5-dione 4-[(3-methoxyphenyl)hydrazone]; ***A11:*** (4Z)-3-methyl-1-(4-nitrobenzoyl)-1H-pyrazole-4,5-dione 4-[(4-bromophenyl)hydrazone]; ***A12:*** (4Z)-3-methyl-1-(4-nitrobenzoyl)-1H-pyrazole-4,5-dione 4-[(2,4-dinitrophenyl)hydrazone]; ***A13:*** (4Z)-3-methyl-1-(4-nitrobenzoyl)-1H-pyrazole-4,5-dione 4-[(2-chloro-4-nitrophenyl)hydrazone]; ***A14:*** (4Z)-3-methyl-1-(4-nitrobenzoyl)-1H-pyrazole-4,5-dione 4-[(4-methyl-2-nitrophenyl)hydrazone]; ***B1:*** (4Z)-1-(2-furoyl)-3-methyl-1H-pyrazole-4,5-dione 4-[(2-nitrophenyl)hydrazone]; ***B2:*** (4Z)-1-(2-furoyl)-3-methyl-1H-pyrazole-4,5-dione 4-[(4-nitrophenyl) hydrazone]; ***B3:*** (4Z)-1-(2-furoyl)-3-methyl-1H-pyrazole-4,5-dione 4-[(2-methyl-4-nitrophenyl)hydrazone]; ***B4:*** (4Z)-1-(2-furoyl)-3-methyl-1H-pyrazole-4,5-dione 4-[(2-chlorophenyl)hydrazone]; ***B5:*** (4Z)-1-(2-furoyl)-3-methyl-1H-pyrazole-4,5-dione 4-[(4-chlorophenyl)hydrazone]; ***B6:*** (4Z)-1-(2-furoyl)-3-methyl-1H-pyrazole-4,5-dione 4-[(3,4-dichlorophenyl)hydrazone]; ***B7:*** (4Z)-1-(2-furoyl)-3-methyl-1H-pyrazole-4,5-dione 4-[(3-chloro-2-methylphenyl) hydrazone]; ***B8:*** (4Z)-1-(2-furoyl)-3-methyl-1H-pyrazole-4,5-dione 4-[(4-fluorophenyl)hydrazone]; ***B9:*** (4Z)-1-(2-furoyl)-3-methyl-1H-pyrazole-4,5-dione 4-[(3-chloro-4-fluorophenyl)hydrazone]; ***B10:*** (4Z)-1-(2-furoyl)-3-methyl-1H-pyrazole-4,5-dione 4-[(3-methoxyphenyl)hydrazone]; ***B11:*** (4Z)-1-(2-furoyl)-3-methyl-1H-pyrazole-4,5-dione 4-[(4-bromophenyl)hydrazone]; ***B12:*** (4Z)-1-(2-furoyl)-3-methyl-1H-pyrazole-4,5-dione 4-[(2,4-dinitrophenyl)hydrazone]; ***B13:*** (4Z)-1-(2-furoyl)-3-methyl-1H-pyrazole-4,5-dione 4-[(2-chloro-4-nitrophenyl)hydrazone]; ***B14:*** (4Z)-1-(2- pyrazole furoyl)-3-methyl-1H-pyrazole-4,5-dione 4-[(4-methyl-2-nitrophenyl)hydrazone]; ***C1:*** (4Z)-1-(2-fluorobenzoyl)-3-methyl-1H-pyrazole-4,5-dione 4-[(2-nitrophenyl)hydrazone]; ***C2:*** (4Z)-1-(2-fluorobenzoyl)-3-methyl-1H-pyrazole-4,5-dione 4-[(4-nitrophenyl)hydrazone]; ***C3:*** (4Z)-1-(2-fluorobenzoyl)-3-methyl-1H-pyrazole-4,5-dione 4-[(2-methyl-4-nitrophenyl)hydrazone]; ***C4:*** (4Z)-1-(2-fluorobenzoyl)-3-methyl-1H-pyrazole-4,5-dione 4-[(2-chlorophenyl)hydrazone]; ***C5:*** (4Z)-1-(2-fluorobenzoyl)-3-methyl-1H-pyrazole-4,5-dione 4-[(4-chlorophenyl)hydrazone]; ***C6:*** (4Z)-1-(2-fluorobenzoyl)-3-methyl-1H-pyrazole-4,5-dione 4-[(3,4-dichlorophenyl) hydrazone]; ***C7:*** (4Z)-1-(2-fluorobenzoyl)-3-methyl-1H-pyrazole-4,5-dione 4-[(3-chloro-2-methylphenyl)hydrazone]; ***C8:*** (4Z)-1-(2-fluorobenzoyl)-3-methyl-1H-pyrazole-4,5-dione 4-[(4-fluorophenyl)hydrazone]; ***C9:*** (4Z)-1-(2-fluorobenzoyl)-3-methyl-1H-pyrazole-4,5-dione 4-[(3-chloro-4-fluorophenyl) hydrazone]; ***C10:*** (4Z)-1-(2-fluorobenzoyl)-3-methyl-1H-pyrazole-4,5-dione 4-[(3-methoxyphenyl)hydrazone]; ***C11:*** (4Z)-1-(2-fluorobenzoyl)-3-methyl-1H-pyrazole-4,5-dione 4-[(4-bromophenyl)hydrazone]; ***C12:*** (4Z)-1-(2-fluorobenzoyl)-3-methyl-1H-pyrazole-4,5-dione 4-[(2,4-dinitrophenyl)hydrazone]; **C13:** (4Z)-1-(2-fluorobenzoyl)-3-methyl-1H-pyrazole-4,5-dione 4-[(2-chloro-4-nitrophenyl)hydrazone]; ***C14:*** (4Z)-1-(2-fluorobenzoyl)-3-methyl-1H-pyrazole-4,5-dione 4-[(4-methyl-2-nitrophenyl)hydrazone]\

Table 1: ADME profile of Pyrazolone derivatives

Structure ID	*Molecular Weight*	*CNS activity*	*DLS*	*Dipole moment*	*HBA*	*QP log O/W*	*NLMR*	*Number of Violations*	*% Human oral absorption*
A1	396.31	-2	2	14.38	7	1.84	5	1	50.058
A2	396.31	-2	1	6.227	7	1.7	4	1	44.59
A3	410.34	-2	1	5.593	7	2.049	5	1	48.616
A4	385.76	-2	1	11.67	6	2.922	4	0	82.495
A5	385.76	-2	1	9.083	6	2.961	3	0	81.442
A6	420.2	-2	1	8.508	6	3.399	3	0	83.989
A7	399.78	-2	1	9.826	6	3.252	5	0	85.181
A8	369.3	-2	1	8.894	6	2.695	3	0	79.885
A9	403.75	-2	1	8.371	6	3.164	3	0	82.627
A10	381.34	-2	0	9.803	6.75	2.514	5	0	78.83
A11	430.21	-2	1	8.758	6	3.041	3	0	81.905
A12	441.31	-2	4	10.946	8	1.085	5	1	29.199
A13	430.75	-2	1	7.583	7	2.166	4	1	48.612
A14	410.34	-2	2	14.879	7	2.167	5	1	52.056
B1	341.27	-2	1	3.761	6.5	1.796	5	0	78.091
B2	341.27	-2	1	12.386	6.5	1.639	4	0	72.337
B3	355.3	-2	1	8.503	6.5	1.988	5	0	76.356
B4	330.72	0	1	11.492	5.5	2.856	4	0	100
B5	330.72	0	0	6.232	5.5	2.9	3	0	96.226
B6	365.17	0	0	7.112	5.5	3.426	3	0	100
B7	344.75	0	0	7.449	5.5	3.189	5	0	100
B8	314.27	0	0	6.098	5.5	2.635	3	0	94.675
B9	348.71	0	0	7.365	5.5	3.122	3	0	100
B10	326.3	-1	0	7.509	6.25	2.457	5	0	93.644
B11	375.17	0	0	6.132	5.5	2.98	3	0	96.694
B12	386.27	-2	0	8.659	7.5	1.041	5	1	44.131
B13	375.72	-2	1	7.268	6.5	2.105	4	0	76.356
B14	355.3	-2	1	7.695	6.5	2.122	5	0	79.969
C1	369.3	-2	1	12.078	6	2.793	4	0	86.12
C2	369.3	-2	2	14.38	6	2.655	3	0	80.491
C3	383.33	-2	1	6.227	6	3.003	4	0	84.476
C4	358.75	0	1	5.593	5	3.889	3	0	100
C5	358.75	0	1	11.67	5	3.917	2	0	100
C6	393.19	0	1	9.083	5	4.358	2	0	100
C7	372.78	0	1	8.508	5	4.204	4	0	100
C8	342.29	0	1	9.826	5	3.638	2	0	100
C9	376.74	0	1	8.894	5	4.12	2	0	100
C10	354.33	0	1	8.371	5.75	3.469	4	0	100
C11	403.2	0	0	9.803	5	3.999	2	0	100
C12	414.3	-2	1	8.758	7	2.037	4	1	52.183
C13	403.75	-2	4	10.946	6	3.122	3	0	84.528
C14	383.3333	-2	1	7.583	6	3.119	4	0	88.012

CNS: Central Nervous System, NHBA: Number of hydrogen bond acceptor, NLMR: Number of Likely metabolic reactions.

Molecular Mechanics Poisson Boltzmann Surface Area (MMPBSA) Analysis

The gmx_MMPBSA programme was used to study the energy decomposition by residues. The MMPBSA run was performed for 100 frames from a total of ten thousand with an interval of a hundred. The total energy decomposition by each residue during the MD run was retrieved during the MMPBSA run. The MMPBSA_ana module was used to visualize the results obtained from the gmx_MMPBSA run.[24]

RESULTS

ADME Profile and Drug Likeness Score

The ADME profile of the test agents was analyzed using the QuickProp module of Schrodinger where we predicted that 34 compounds did not violate Lipinski's rule of five (Table 1). However, 8 compounds were predicted to violate one rule. Oral absorption was predicted, where 11 compounds (B4, B6, B9, C4-11) were predicted to be completely absorbed via the oral route. Similarly, 15 compounds (A4, A5, A6, A7, A9, A11, B5, B8, B10, B11, C1, C2, C3, C13, C14) were predicted to possess an oral absorptivity greater than 80%. The test agent A14 owned the highest dipole moment of 14.879. In contrast, B1 was predicted to possess the lowest dipole moment of 3.761. Moreover, 15 compounds (B4-B9, B11, C4-C11) were predicted to acquire a positive CNS activity score along with a QPlog O/W score greater than 2.5 indicating their probability of crossing the BBB. Additionally, A12 anticipated to possess the high no. of hydrogen bond donors, i.e., 8. The drug-likeness score revealed that the compounds A12 and C13 possessed the highest DLS of 4; whereas the compounds A1, A14, and C2 possessed the DLS of 2, and compounds A2-A9, A11, A13, B1-B4, B13, B14, C1, C3-C10, C12-C14 possessed a DLS of 1 (Table 1).

Adverse Reaction and Biological Spectra Prediction

Adverse effects for the test agents were predicted via the ADVERPred database, where we predicted 26 compounds possessed a side effect of hepatotoxicity. The compound A9 anticipated to possess the maximum pharmacological activity of 0.691. On the contrary, C5 and C8 possessed the lowest pharmacological activity of 0.331 (Table 2).

Table 2: Prediction of biological spectra for pyrazolone derivatives against parkinson's disease

Structure code	*Pa*	*Pi*	*Biological Spectra*
A1	0.07	0.021	Bcl-xL inhibitor
	0.117	0.08	Bcl2 antagonist
A2	0.05	0.042	Catechol O methyltransferase inhibitor
A3	0.054	0.034	Catechol O methyltransferase inhibitor
A8	0.048	0.047	Catechol O methyl transferase inhibitor
A9	0.048	0.047	Catechol O methyl transferase inhibitor
A12	0.068	0.025	Bcl-xL inhibitor
	0.113	0.103	Bcl2 antagonist
A14	0.072	0.019	Bcl-xL inhibitor
	0.12	0.069	Bcl2 antagonist
	0.054	0.035	Catechol O methyl transferase inhibitor
B1	0.071	0.02	Bcl-xL inhibitor
	0.112	0.11	Bcl2 antagonist
B3	0.048	0.047	Catechol O methyl transferase inhibitor
B10	0.056	0.052	MAO B inhibitor
B11	0.068	0.024	Bcl-xL inhibitor
B12	0.068	0.024	Bcl-xL inhibitor
	0.097	0.096	Caspase 3 inhibitor
B14	0.072	0.019	Bcl-xL inhibitor
	0.115	0.091	Bcl2 antagonist
C1	0.067	0.026	Bcl-xL inhibitor
	0.115	0.093	Bcl2 antagonist
C3	0.051	0.041	Catechol O methyl transferase inhibitor
C14	0.069	0.023	Bcl-xL inhibitor
	0.118	0.079	Bcl2 antagonist
	0.049	0.045	Catechol O methyl transferase inhibitor

Table 3: Side effects predicted for the series along with their Pharmacological activity and inactivity

Compound Id	*Pharmacological activity*	*Pharmacological inactivity*	*Side Effect*
A1	0.417	0.246	Hepatotoxicity
A2	0.416	0.247	Hepatotoxicity
A3	0.434	0.234	Hepatotoxicity
A4	0.519	0.185	Hepatotoxicity
A5	0.471	0.211	Hepatotoxicity
A6	0.482	0.205	Hepatotoxicity
A7	0.428	0.238	Hepatotoxicity
A8	0.635	0.127	Hepatotoxicity
A9	0.691	0.103	Hepatotoxicity
A10	0.328	0.324	Hepatotoxicity
A11	0.685	0.106	Hepatotoxicity
A12	0.453	0.222	Hepatotoxicity
A13	0.539	0.175	Hepatotoxicity
A14	0.432	0.236	Hepatotoxicity
C1	0.394	0.263	Hepatotoxicity
C2	0.446	0.227	Hepatotoxicity
C3	0.465	0.215	Hepatotoxicity
C4	0.359	0.291	Hepatotoxicity
C5	0.331	0.32	Hepatotoxicity
C6	0.338	0.313	Hepatotoxicity
C8	0.331	0.321	Hepatotoxicity
C9	0.379	0.275	Hepatotoxicity
C11	0.495	0.198	Hepatotoxicity
C12	0.486	0.203	Hepatotoxicity
C13	0.582	0.153	Hepatotoxicity
C14	0.409	0.252	Hepatotoxicity

Molecular Docking

The compound C13 possessed the highest binding affinity of -7.81, with TRAP-1 possessing one hydrogen bond with Asn371, 2 π-π stacking with Trp333, and 1 salt-bridge with Asp122. Compound C12 displayed the highest binding energy of -3.15 with the receptor D2 owing 2 hydrogen bonds with Gln373, and Arg220, 1 π-cation with Arg220, and 1 salt-bridge with Arg1096. The compound C14 possessed the highest binding affinity of -8.49, with the D1 receptor displaying 1 hydrogen bond with Cys198, 2 π-cation with Lys81 & Trp90, and 1 π-π stacking with Trp99. The compound A1 Showed the highest binding affinity of -3.43, with the protein Bcl-XL possessing 1 π-cation with Glu98, and 5 salt bridges with Lys20, Asp95, and Glu98. The compound C9 owned the highest binding affinity of -6.09 with the protein Bax containing 1 hydrogen bond with Gly160 and 1 π-π staking with Trp151. The compound C7 displayed the highest binding affinity of -2.77, with the protein Caspase 3 possessing 2 hydrogen bonds with Arg164 and Cys64. The compounds A5 and C1 possessed the highest binding affinity of -4.17 with Caspase 9, with both the ligands possessing two hydrogen bonds with residue Thr308 and one π-π stacking with Trp310.

The compound C13 displayed the highest binding affinity of -9.78 with MAO-B possessing 2 hydrogen bond interactions; Ile14 and oxygen present at position 20 AND Gly343 and nitrogen present at position 18 and 1 salt bridge interaction; Arg 42 and oxygen present at position 27 (Figure 4) (Supplementary file 1).

Molecular Dynamic Simulation

On completion of the MD run, the RMSD value was analysed for the backbone and complex, which was not stable up to 10 ns and possessed fluctuation between 1 Å to 2.8 Å. However, after 10 ns, the RMSD of the complex and backbone became stable with a fluctuation range of 0.5 Å. Similarly, the RMSF value fluctuated 3 Å throughout the simulation, indicating the residues to be stable. The radius of gyration analysis displayed a fluctuation in the range of 0.25 Å throughout the MD run; there was a spike increase in Rg value at 12 ns, after which it remained constant. Solvent-accessible-surface-area found to be in range of 215 to 230 nm^3 indicating the sufficient surface being available for the ligand to bind with the protein. Moreover, we also analysed the no. of hydrogen bonds fashioned throughout the simulation; it displayed a constant of

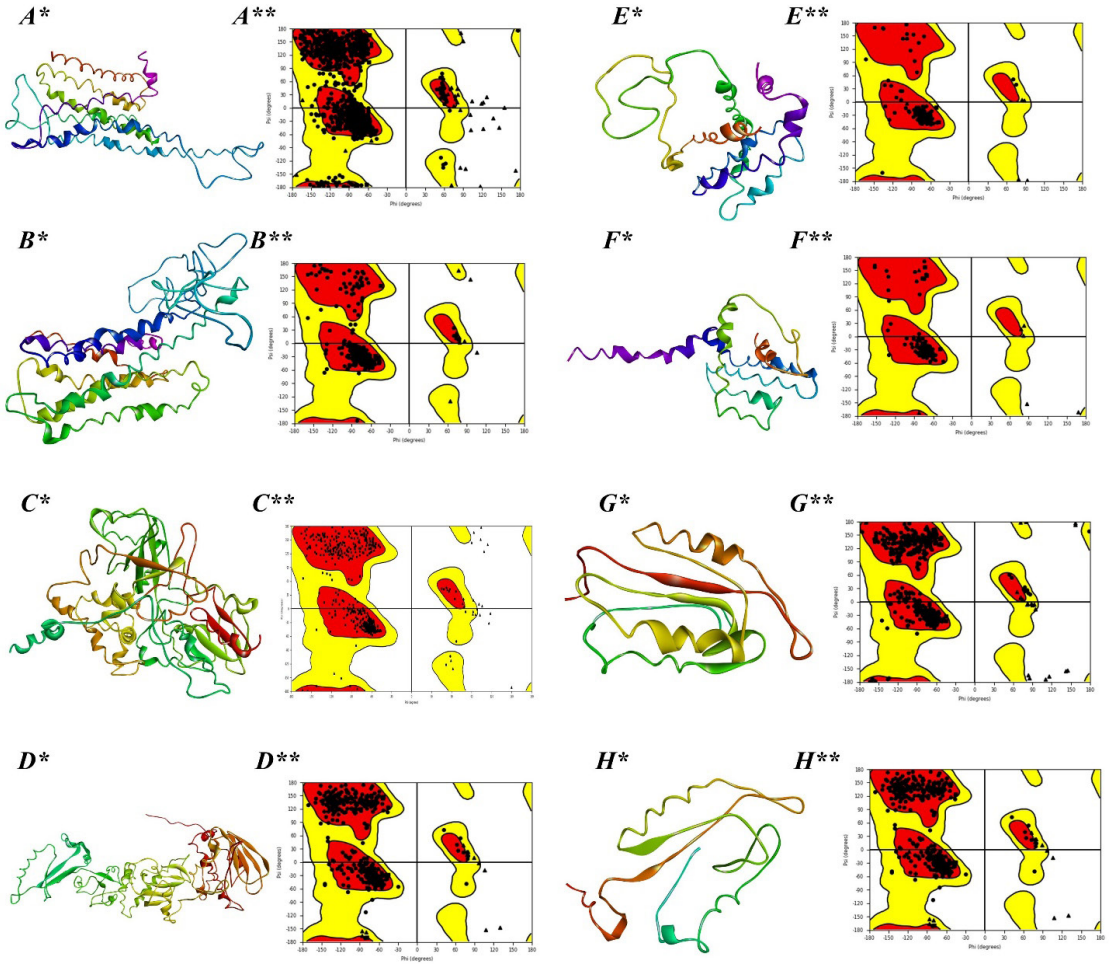

Figure 2: Represents the 3D structure of protein along with their Ramachandran plot. Where, * 3D protein structures; **Ramachandran plot for the proteins. (A) Dopamine receptor-1 (7JOZ); (B) Dopamine receptor-2 (6CM4); (C) Mono Amino Oxidase-B (2V5Z); (D) TRAP-1 (4Z1F); (E) BCL_XL (3SP7); (F) BAX (4BD2); (G) CASP 3 (1CP3); (H) CASP 9 (1NW9).

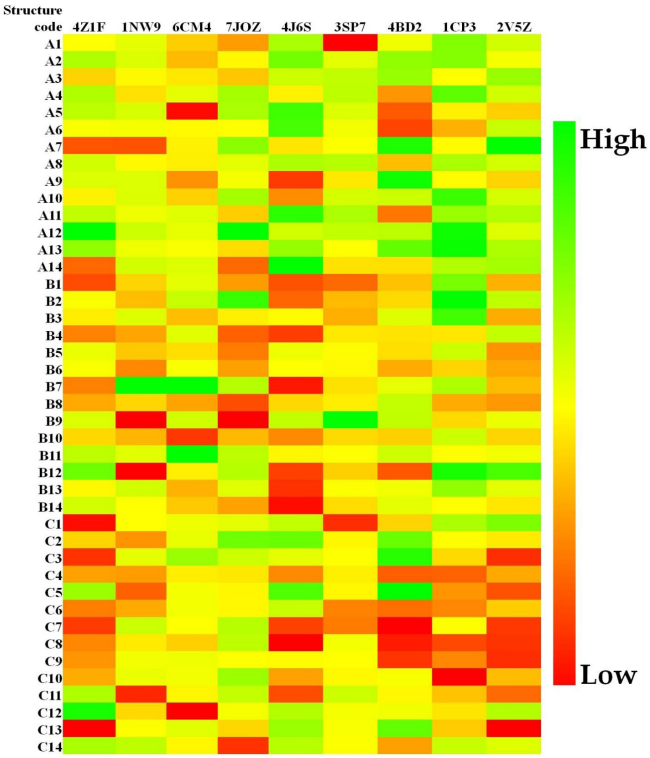

Figure 3: Docking score of pyrazolone derivatives with respective proteins involved in the pathogenesis of Parkinson's disease.

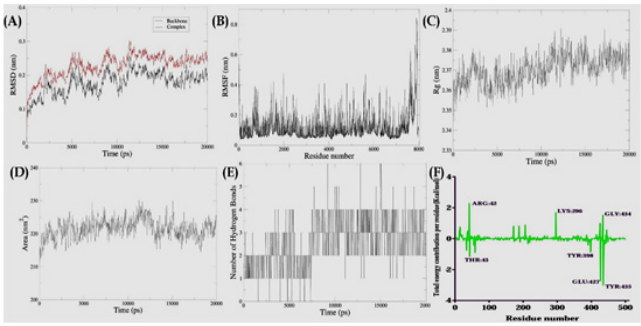

Figure 5: The parameters describing MAO-B vs C13 complex structural stabilities such as RMSD of backbone and complex (A), RMSF (B), Radius of gyration (C), and Solvent accessible surface area (D) are shown. The number of H-bonding interactions (E) formed during the MD. Total energy contribution with residue number (F) formed during the MMPBSA.

2 hydrogen bonds for the starting 7–8 ns thereafter, there was an increase in the number of hydrogen bonds to 3 and constant till 20 ns indicating better stability of the ligand protein complex. There was a maximum of 6 hydrogen bonds visible at 15 ns; this may be due to glutamic acid and tyrosine, which may have fashioned a hydrogen bond with ligand (Figure 5).

Molecular Mechanics Poisson-Boltzmann Surface Area (MMPBSA) Analysis

MMPBSA analysis displayed a total of -2.69 kcal/mol Van der Waal force throughout the MD run, and the electrostatic molecular mechanics was perceived to be -78.45 kcal/mol. Similarly, the total solvation energy was found to be -36.55

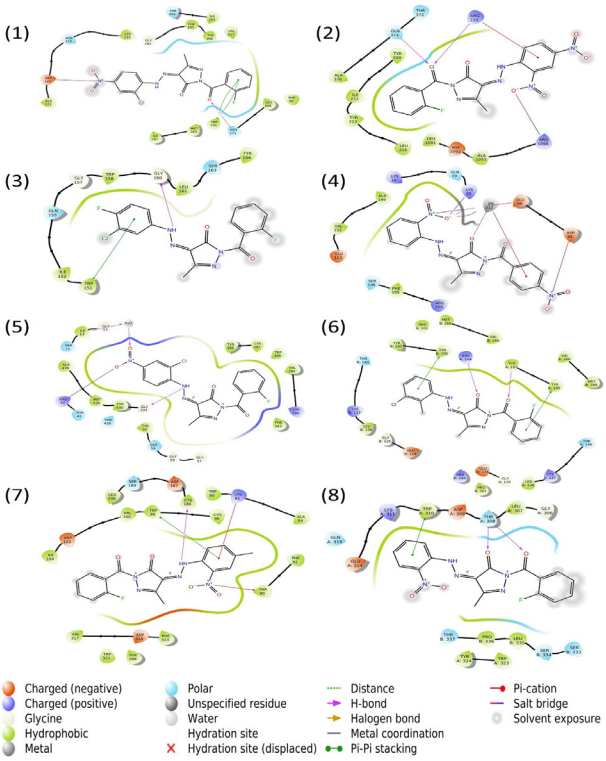

Figure 4: 2-D interactions with test compound & proteins with highest binding score: (1) TRAP-1 (4Z1F) with C13; (2) Dopamine receptor-2 (6CM4) with C12; (3) BAX (4BD2) with C9; (4) BCL_XL (3SP7) withA1; (5) Mono Amino Oxidase-B (2V5Z) with C13; (6) CASP 3 (1CP3) with C7; (7) Dopamine receptor-1 (7JOZ) with C14; (8) CASP 9 (1NW9) with A5 & C1.

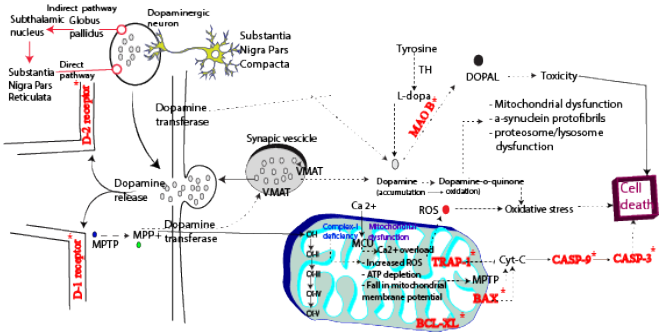

Figure 6: Proteins involved in the pathogenesis of parkinson's disease . Where, BAX: Bcl-2 Associated X-protein; BCL-XL: B-cell lymphoma-extra-large; CASP-3: caspase3; CASP-9: caspase9; Cyt-C: Cytochrome-C; DOPAL: 3,4-Dihydroxyphenylacetaldehyde; MAO-B: Mono Amino Oxidase-B; MPP+: 1-methyl-4-phenylpyridinium; MPTP: 1-methyl-4-phenyl-1,2,3,6-tetrahydropyridine; ROS: reactive oxygen species; TRAP-1: Tumor Necrosis Factor-Associated Protein1; VMAT: Vesicular monoamine transporter.

kcal/mol. Moreover, upon calculation of energy contribution per residue, it was found that tyrosine 435 possessed the least total binding contribution with the ligand, *i.e.,* -3.02 kcal/mol indicating it to be in favour of binding. In addition, the residues Glu427, Tyr398, and Thr43 favoured the simulation possessing a total energy contribution of -2.75, 0.86, and -1.15 kcal/mol, respectively. However, the residues Arg42, Lys296,

and Gly434 possessed positive energy contributions with total energy contributions of 2.29, 1.69, and 1.53 kcal/mol, respectively (Figure 6).

DISCUSSION

Parkinson's disease is a major clinical challenge due to the lack of appropriate diagnosis since symptoms vary from person to person. The typical clinical manifestations involved are bradykinesia, akinesia, and postural instability resulting from reduced dopamine levels at SNPC, which may be due to the increased metabolism of dopamine or the deposition of α-synuclein in the neuronal cells.[25] The absence of standard therapy for PD in the current scenario, urged us to look upon pyrazolone derivatives which are known to possess neuromodulatory effect via antioxidant and *in-vitro* MAO -B inhibitory activity.[26]

Various proteins are responsible for modulation of disease condition. Dopamine receptors for regulating dopamine via G protein-coupled receptor (GPCR) that induce stimulation of adenylyl cyclase (AC) activity and play a vital role in regulating behavioural activity like locomotor activity, reward system, memory and, learning through D1 receptors. The D2 receptor inhibits AC activation, reducing cAMP levels, which plays an essential part in the postsynaptic behavioural response mediated by receptors as well as extra-pyramidal activity. In addition, DA2 receptors are auto receptors which are acknowledged to reduction of neuronal impulsiveness and reduce dopamine synthesis and release in Parkinson's disease. PINK-1 protein has an important part in regulating trap-1 and Bcl-xL genes involved in the pathogenesis of PD.[27] Upon phosphorylation, they inhibit Cytochrome-C (Cyt-C) release and autophagy, respectively. TRAP-1 works as a chaperon to improve the molecular level functioning of mitochondria by eradicating misfolded and misassembled proteins. Further apoptotic stimuli trigger pro-apoptotic protein BAX responsible for initiating membrane permeability in mitochondria that releases Cyt-C and forms a complex with an Apoptotic protease activating factor-1 (Apaf-1) which mobilizes procaspase-9 activation via proteolysis to form caspase 9. Further, caspase-9 promotes executioner caspases-3 to regulate proteolysis leading to apoptosis.[28]

The primary treatment approach for PD is levodopa with MAO-B inhibition. Biogenic amines like dopamine are catalysed by oxidative deamination by this enzyme. MAOs are confined in the peripheral membrane of mitochondria carrying out metabolism of neuroactive monoamines in CNS such as dopamine (DA), norepinephrine, serotonin, and melatonin. Among the various monoamine neurotransmitters, DA gets degraded by MAO-A and MAO-B. Dopamine neurons take up the accumulated dopamine from the synaptic cleft, which is further degraded by MAO and Catechol-O-methyl transferase (COMT). MAO-B is thought to be more prominently involved in DA degradation due to the positive therapeutic effect of MAO-B inhibitors in PD patients.[29] Therefore, modulating these protein targets during disease conditions can give significant outcomes to combat PD conditions.

In the present study, we have designed novel pyrazolone derivatives and utilized multiple in-silico tools to predict the potential for anti-Parkinson's activity. The pharmacokinetic predictions revealed that the majority of compounds obeyed Lipinski's rule of five. In addition, compounds were predicted to own oral absorptivity greater than 80%, suggesting that they can be used orally. This reinforces our study since patients with Parkinson's disease are often on long-term medications, making the oral route the most convenient route of administration. Moreover, 15 compounds were predicted to possess PLog oil in water ratio to be more than 2.5, indicating the ability to cross the blood-brain barrier; the compounds containing 2-flurobenzoichydrazide , *i.e.,* category C, possessed the highest oil in water ratio. In addition, we also predicted the side effects which the compounds may cause, and the majority of compounds showed tendency of hepatotoxicity.

Furthermore, *in-silico* molecular docking studies provided insights and predicted the binding affinity and intermolecular interactions of the synthesized compounds with proteins. In this regard, Compound C13 possessed the highest binding affinity and stable interactions with the MAO-B which may prove beneficial role in Parkinson's disease. In addition, C13 possessed the highest DLS with negligible adverse effects and the highest biological spectrum for catalase stimulation. This study adds value to the previously reported data regarding neuromodulation property of pyrazolone derivative, Edaravone,[30,31] which can be further investigated using *in-vitro* and *in-vivo* experimental studies.

CONCLUSION

We have designed substituted pyrazolone moieties and with the support of computer aided drug design, performed screening for anti-Parkinson's activity with potential to inhibit = numerous proteins involved in disease modulation. The eight targets identified in our study that are involved in the pathogenesis of PD were TRAP-1, MAO-B, D1, D2, Bcl-xL, BAX, CASP3 and CASP9. The involvement of MAO-B in the maintenance of dopamine levels through methylation is significant. *In-silico* docking results predicted significant affinities of pyrazolone derivatives with MAO-B. Also it is interesting to note the interaction of these newly designed molecules with targets like Bcl-xL, BAX, CASP3 and CASP9 which may contribute favourable pharmacological action by slowing down or decreasing neuronal degeneration. Therefore the present study revealed that substituted novel pyrazolone derivatives can serve as a promising lead moiety for developing anti-Parkinson's agents.

Availability of Data and Materials

The datasets generated during and/or analysed during the current study are available from the corresponding author Harsha Ashtekar (hrshshtkr2@gmail.com) on reasonable request.

ACKNOWLEDGEMENT

The authors extend their thankfulness to Institute for providing CADD lab facility with Schrodinger software

REFERENCES

1. Leão AH, Meurer YS, da Silva AF, Medeiros AM, Campêlo CL, Abílio VC, Engelberth RC, Cavalcante JS, Izídio GS, Ribeiro AM, Silva RH. Spontaneously hypertensive rats (SHR) are resistant to a reserpine-induced progressive model of Parkinson's disease: Differences in motor behavior, tyrosine hydroxylase and α-synuclein expression. Frontiers in aging neuroscience. 2017 Mar 27;9:78.
2. Gubellini P, Kachidian P. Animal models of Parkinson's disease: An updated overview. Revue neurologique. 2015 Nov 1;171(11):750-61.
3. Oswal A, Cao C, Yeh CH, Neumann WJ, Gratwicke J, Akram H, Horn A, Li D, Zhan S, Zhang C, Wang Q. Neural signatures of hyperdirect pathway activity in Parkinson's disease. Nature communications. 2021 Aug 31;12(1):5185.
4. Church FC. Treatment options for motor and non-motor symptoms of Parkinson's disease. Biomolecules. 2021 Apr 20;11(4):612.
5. Merugumolu VK, Chandrashekara RB. Synthesis and anti-depressant evaluation of novel pyrazolone derivatives. Bangladesh Journal of Pharmacology. 2016 May 25;11(2):558-63.
6. Prajuli R, Banerjee J, Khanal HE. Synthesis of some pyrazolone derivatives and evaluation of its antibacterial and cytotoxic activity. Oriental Journal of Chemistry. 2015 Dec 1;31(4):2099-106.
7. Abdellattif MH, Shahbaaz M, Arief MM, Hussien MA. Oxazinethione derivatives as a precursor to pyrazolone and pyrimidine derivatives: Synthesis, biological activities, molecular modeling, ADME, and molecular dynamics studies. Molecules. 2021 Sep 9;26(18):5482.
8. Herbet M, Natorska-Chomicka D, Ostrowska M, Gawrońska-Grzywacz M, Izdebska M, Piątkowska-Chmiel I, Korga A, Wróbel A, Dudka J. Edaravone presents antidepressant-like activity in corticosterone model of depression in mice with possible role of Fkbp5, Comt, Adora1 and Slc6a15 genes. Toxicology and Applied Pharmacology. 2019 Oct 1;380:114689.
9. Klutzny S, Kornhuber M, Morger A, Schoenfelder G, Volkamer A, Oelgeschlaeger M, Dunst S. Quantitative high-throughput phenotypic screening for environmental estrogens using the E-Morph Screening Assay in combination with in silico predictions. Environment International. 2022 Jan 1;158:106947.
10. Li Y, Qiu L, Liu X, Hou Z, Yu B. PINK1 alleviates myocardial hypoxia-reoxygenation injury by ameliorating mitochondrial dysfunction. Biochemical and biophysical research communications. 2017 Feb 26;484(1):118-24.
11. Mathew GE, Oh JM, Mohan K, Tengli A, Mathew B, Kim H. Development of methylthiosemicarbazones as new reversible monoamine oxidase-B inhibitors for the treatment of Parkinson's disease. Journal of Biomolecular Structure and Dynamics. 2021 Sep 2;39(13):4786-94.
12. Leão RP, Cruz JV, da Costa GV, Cruz JN, Ferreira EF, Silva RC, de Lima LR, Borges RS, Dos Santos GB, Santos CB. Identification of new rofecoxib-based cyclooxygenase-2 inhibitors: A bioinformatics approach. Pharmaceuticals. 2020 Aug 26;13(9):209.
13. Poroikov VV, Filimonov DA, Ihlenfeldt WD, Gloriozova TA, Lagunin AA, Borodina YV, Stepanchikova AV, Nicklaus MC. PASS biological activity spectrum predictions in the enhanced open NCI database browser. Journal of chemical information and computer sciences. 2003 Jan 27;43(1):228-36.
14. Ivanov SM, Lagunin AA, Rudik AV, Filimonov DA, Poroikov VV. ADVERPred–Web service for prediction of adverse effects of drugs. Journal of Chemical Information and Modeling. 2018 Jan 22;58(1):8-11.
15. Dwivedi PS, Rasal VP, Kotharkar E, Nare S, Khanal P. Gene set enrichment analysis of PPAR-γ regulators from Murraya odorata Blanco. Journal of Diabetes & Metabolic Disorders. 2021 Jun;20:369-75.
16. Dwivedi PS, Patil VS, Khanal P, Bhandare VV, Gurav S, Harish DR, Patil BM, Roy S. System biology-based investigation of Silymarin to trace hepatoprotective effect. Computers in biology and medicine. 2022 Mar 1;142:105223.
17. Chi H, Jain H. Teaching computing to STEM students via visualization tools. Procedia Computer Science. 2011 Jan 1;4:1937-43.
18. Gahlawat A, Kumar N, Kumar R, Sandhu H, Singh IP, Singh S, Sjöstedt A, Garg P. Structure-based virtual screening to discover potential lead molecules for the SARS-CoV-2 main protease. Journal of chemical information and modeling. 2020 Jul 20;60(12):5781-93.
19. Shah B, Modi P, Sagar SR. In silico studies on therapeutic agents for COVID-19: Drug repurposing approach. Life sciences. 2020 Jul 1;252:117652.
20. Rajagopal K, Varakumar P, Aparna B, Byran G, Jupudi S. Identification of some novel oxazine substituted 9-anilinoacridines as SARS-CoV-2 inhibitors for COVID-19 by molecular docking, free energy calculation and molecular dynamics studies. Journal of Biomolecular Structure and Dynamics. 2021 Sep 2;39(15):5551-62.
21. Moumbock AF, Li J, Tran HT, Hinkelmann R, Lamy E, Jessen HJ, Günther S. ePharmaLib: a versatile library of e-pharmacophores to address small-molecule (poly-) pharmacology. Journal of Chemical Information and Modeling. 2021 Jul 8;61(7):3659-66.
22. Leis S, Zacharias M. Efficient inclusion of receptor flexibility in grid-based protein–ligand docking. Journal of Computational Chemistry. 2011 Dec;32(16):3433-9.
23. Khanal P, Patil VS, Bhandare VV, Dwivedi PS, Shastry CS, Patil BM, Gurav SS, Harish DR, Roy S. Computational investigation of benzalacetophenone derivatives against SARS-CoV-2 as potential multi-target bioactive compounds. Computers in Biology and Medicine. 2022 Jul 1;146:105668.
24. Betsch C, Schmid P, Heinemeier D, Korn L, Holtmann C, Böhm R. Beyond confidence: Development of a measure assessing the 5C psychological antecedents of vaccination. PloS one. 2018 Dec 7;13(12):e0208601.
25. Ninkina N, Tarasova TV, Chaprov KD, Roman AY, Kukharsky MS, Kolik LG, Ovchinnikov R, Ustyugov AA, Durnev AD, Buchman VL. Alterations in the nigrostriatal system following conditional inactivation of α-synuclein in neurons of adult and aging mice. Neurobiology of Aging. 2020 Jul 1;91:76-87.
26. Chimenti F, Bolasco A, Manna F, Secci D, Chimenti P, Befani O, Turini P, Giovannini V, Mondovì B, Cirilli R, La Torre F. Synthesis and selective inhibitory activity of 1-acetyl-3, 5-diphenyl-4, 5-dihydro-(1 H)-pyrazole derivatives against monoamine oxidase. Journal of medicinal chemistry. 2004 Apr 8;47(8):2071-4.
27. Mishra A, Singh S, Shukla S. Physiological and functional basis of dopamine receptors and their role in neurogenesis: possible implication for Parkinson's disease. Journal of experimental neuroscience. 2018 May 31;12:1179069518779829.
28. Erekat NS. Apoptosis and its Role in Parkinson's Disease. Exon Publications. 2018 Dec 21:65-82.
29. Cho HU, Kim S, Sim J, Yang S, An H, Nam MH, Jang DP, Lee CJ. Redefining differential roles of MAO-A in dopamine degradation and MAO-B in tonic GABA synthesis. Experimental & Molecular Medicine. 2021 Jul;53(7):1148-58.
30. Minnelli C, Laudadio E, Galeazzi R, Rusciano D, Armeni T, Stipa P, Cantarini M, Mobbili G. Synthesis, characterization and antioxidant properties of a new lipophilic derivative of edaravone. Antioxidants. 2019 Jul 31;8(8):258.
31. Cha SJ, Kim K. Effects of the edaravone, a drug approved for the treatment of amyotrophic lateral sclerosis, on mitochondrial function and neuroprotection. Antioxidants. 2022 Jan 20;11(2):195.